Numerical Simulation for Gas-Liquid Two-Phase Free Turbulent Flow Based on Vortex in Cell Method*

Tomomi UCHIYAMA** and Tomohiro DEGAWA***

This paper proposes a two-dimensional vortex method, based on Vortex in Cell method, for gas-liquid two-phase free turbulent flow. The behavior of vortex element and the bubble motion are calculated through the Lagrangian approach, while the change in the vorticity due to the bubble is analyzed in the computational grids resolving the flow field. Therefore, the numerical procedure corresponds to the Lagrangian-Eulerian method. The present method is applied to simulate the air-water bubbly flow around a square-section cylinder. The simulation demonstrates that the bubble entrainment into the Karman vortex and the resultant reduction for the strength of vortex are successfully captured by the method. It is also confirmed that the vortex shedding frequency and the pressure distribution on the cylinder are favorably compared with the measured results.

Key Words: Multiphase Flow, Numerical Analysis, Vortex Method, Bubbly Flow, Wake

1. Introduction

Free turbulent flows loaded with small bubbles are observed in various engineering applications including chemical reactors, heat exchangers and waste treatment systems. For the fundamental flows, such as plane mixing layers[1),(2)], jet[3)] and wake flows behind an obtuse body[4)-(6)], the turbulence modulation of the liquid-phase due to the bubble and the relation between the large-scale vortical structure and the bubble motion have been experimentally investigated. Some numerical analyses have also been carried out. Sun and Faeth[7)] simulated the jet, issuing from a round nozzle, by using a k-ε turbulence model based on the steady and axisymmetrical assumptions. They reported that the velocity and the gas volumetric fraction are favorably predicted by the model. Sugiyama et al.[8)] developed a finite difference method employing a number density model for bubble, and they analyzed the bubbly flow around a circular cylinder to investigate the phase distribution and the behavior of the Karman vortex. To make clear the flow field in detail, direct numerical simulations on mixing layers have been performed. Ruetsch and Meiburg[9)] reported that the accumulation of bubble on the higher vorticity region, called the preferential concentration of bubble, reduces the vorticity and the pressure gradient. Druzhinin and Elghobashi[10)] clarified the bubble accumulation caused by the merging of the large-scale eddies.

Recently, vortex methods have been usefully applied to analyze single-phase free turbulent flows. This is because the methods can simulate directly the development of vortical structure, such as the formation and deformation of vortices, through the Lagrangian calculation for the behavior of the vortex elements discretizing the vorticity field. To extend the applicability of vortex methods, one of the authors[11),(12)] has proposed the vortex methods for gas-particle two-phase free turbulent flow. The methods were applied to simulate various free turbulent flows[13)-(17)]. Uchiyama and Naruse[18)] proposed another two-dimensional vortex method for gas-particle free turbulent flow. The method is based on the Vortex in Cell method, abbreviated to VIC method, presented for the single-phase flow analysis. It can calculate the convection velocity of vortex element with less CPU time than the former vortex method.

Since the free turbulent flow entraining small bubbles is chiefly governed by the large-scale eddies of the liquid-phase, the vortex method promises to be applicable to simulate the flow. Such two-phase vortex method has been rarely presented except for few studies, in which

* Received 23rd February, 2006 (No. 05-0741). Japanese Original: Trans. Jpn. Soc. Mech. Eng., Vol.72, No.718, B (2006), pp.1418–1425 (Received 12th July, 2005)

** EcoTopia Science Institute, Nagoya University, Furo-cho, Chikusa-ku, Nagoya 464–8603, Japan.
E-mail: uchiyama@is.nagoya-u.ac.jp

*** Graduate School of Information Science, Nagoya University, Furo-cho, Chikusa-ku, Nagoya 464–8601, Japan

the flow of liquid-phase is simulated by vortex methods and the bubble motion is computed by the Lagrangian approach. Sene et al.[19] conducted the two-dimensional simulation of the air bubble motion in a plane mixing layer by assuming that the water flow is not affected by the bubbles. By using such one-way scheme, Uchiyama[20] performed the three-dimensional simulation of a bubbly jet to search for the possibility to control the bubble dispersion. Yang et al.[21] proposed a two-dimensional two-way vortex method, which can take account for the interaction between the two phases, to simulate a plane mixing layer loaded with bubbles. But the volumetric fraction is not considered in the conservation equations for the liquid-phase. Thus, the method seems to be unreasonable.

This study proposes a two-dimensional two-way vortex method, based on the VIC method, for gas-liquid two-phase free turbulent flow. In the method, the bubble motion and the behavior of vortex element are traced, while the change in the vorticity due to the bubble is computed in the computational grids resolving the flow field. Therefore, the numerical procedure corresponds to the Lagrangian-Eulerian method. This study also applies the vortex method to simulate the air-water bubbly flow around a square-section cylinder. It is confirmed that the simulated flow fields are favorably compared with the corresponding experiments and the existing numerical results on bubble-laden free turbulent flows.

Nomenclatures

A : area of computational grid
C_p : pressure coefficient $=(p-p_0)/(\rho_m u_m^2/2)$
d : bubble diameter
f : vortex shedding frequency
$\boldsymbol{g}$: gravitational constant
N_v : number of vortex elements in computational domain
n_g : number of bubbles in computational grid
n_v : number of vortex elements in computational grid
p : pressure
Re : Reynolds number $=u_{l0}s/\nu_l$
St : Strouhal number $=fs/u_{l0}$
s : side length for square-section cylinder
t : time
t^* : nondimensional time $=u_{l0}t/s$
$\boldsymbol{u}$: velocity
u_m : volumetric velocity of liquid-phase at inlet boundary
x,y : orthogonal coordinates
α : volumetric fraction
Δp : pressure difference between front and rear stagnation points of cylinder
Δt : time increment
Δz : interval between bubbles in direction normal to x–y plane
Γ : circulation
ν : kinematic viscosity
ρ : density
ρ_m : mean density $=\alpha_{g0}\rho_g+\alpha_{l0}\rho_l$
σ : core radius
ϕ : scalar potential
$\boldsymbol{\psi}$: vector potential
ω : vorticity $=\nabla\times\boldsymbol{u}_l$

Subscripts :

0 : inlet boundary or initial value
g : gas-phase
l : liquid-phase
z : direction normal to x–y plane

2. Basic Equations

2.1 Assumptions

The following assumptions are employed for the simulation.

(1) The mixture is a bubbly flow entraining small bubbles.

(2) Both phases are incompressible and no phase changes occur.

(3) The mass and momentum of the gas-phase are very small and negligible compared with those of the liquid-phase.

(4) The bubbles maintain their spherical shape, and neither fragmentation nor coalescence occurs.

2.2 Conservation equations for bubbly flow

The conservation equations for the mass and momentum of the bubbly flow are expressed by the following equations under the assumptions (1)–(3).

$$\frac{\partial\alpha_l}{\partial t}+\nabla\cdot(\alpha_l\boldsymbol{u}_l)=0 \tag{1}$$

$$\alpha_l\frac{D\boldsymbol{u}_l}{Dt}=-\frac{1}{\rho_l}\nabla p+\nu_l\nabla^2\boldsymbol{u}_l+\alpha_l\boldsymbol{g} \tag{2}$$

where

$$\alpha_g+\alpha_l=1 \tag{3}$$

Since the vortex method proposed by Yang et al.[21] solves Eqs. (1) and (2) with $\alpha_l=1$ and $\alpha_g=0$, the two-way coupling between the two phases is incomplete. This study proposes a vortex method that can take into account the volumetric fraction for each phase.

2.3 Equation of motion for bubble

It is postulated that the virtual mass force, the drag force, the gravitational force and the lift force act on the bubble. In this case, the equation of motion for the bubble is expressed by the following equation under the assumption (4).

$$\frac{d\boldsymbol{u}_g}{dt}=\frac{1+C_V}{\beta+C_V}\frac{D\boldsymbol{u}_l}{Dt}-\frac{1}{\beta+C_V}\frac{3C_D}{4d}\boldsymbol{u}_r|\boldsymbol{u}_r| +\frac{\beta-1}{\beta+C_V}\boldsymbol{g}-\frac{C_L}{\beta+C_V}\boldsymbol{u}_r\times(\nabla\times\boldsymbol{u}_l) \tag{4}$$

where d is the bubble diameter, $\boldsymbol{u}_r = \boldsymbol{u}_g - \boldsymbol{u}_l$ and $\beta = \rho_g/\rho_l$. C_D, C_V and C_L are the drag coefficient, the virtual mass coefficient and the lift coefficient, respectively. C_D is given as[22]:

$$C_D = (24/Re_b)\left(1 + 0.15Re_b^{0.687}\right) \tag{5}$$

where $Re_b = d|\boldsymbol{u}_r|/\nu_l$.

2.4 Decomposition of liquid velocity field

According to the Helmholtz' theorem, any vector field can be represented as the summation of the gradient for a scalar potential ϕ and the rotation for a vector potential $\boldsymbol{\psi}$[23]. Thus, the liquid velocity $\boldsymbol{u}_l$ is written as:

$$\boldsymbol{u}_l = \nabla\phi + \nabla\times\boldsymbol{\psi} \tag{6}$$

The velocity calculated from Eq. (6) remains unaltered even when any gradient of scalar function is added to $\boldsymbol{\psi}$[23]. To remove this arbitrariness, a solenoidal condition is imposed on $\boldsymbol{\psi}$:

$$\nabla\cdot\boldsymbol{\psi} = 0 \tag{7}$$

When substituting Eq. (6) into Eq. (1) and rewriting the resultant equation by using a relation $\nabla\cdot(\nabla\times\boldsymbol{\psi}) = 0$, the following equation is obtained.

$$\frac{\partial\alpha_l}{\partial t} + \nabla\cdot(\alpha_l\nabla\phi) + \nabla\times\boldsymbol{\psi}\cdot\nabla\alpha_l = 0 \tag{8}$$

Taking the rotation of Eq. (6) and substituting Eq. (7) into the resultant equation, the vector Poisson equation is derived:

$$\nabla^2\boldsymbol{\psi} = -\boldsymbol{\omega} \tag{9}$$

where $\boldsymbol{\omega}$ is the vorticity for the liquid-phase.

3. Numerical Method

3.1 Lagrangian analysis for vortex element and bubble

When taking the rotation of Eq. (2), the vorticity equation for the bubbly flow is derived. For the two-dimensional calculation, it is expressed by the following equation.

$$\frac{\partial\omega}{\partial t} + \nabla\cdot(\omega\boldsymbol{u}_l) = \frac{\nu_l}{\alpha_l}\nabla^2\omega + \frac{1}{\alpha_l}\nabla\alpha_l\times\left(\boldsymbol{g} - \frac{D\boldsymbol{u}_l}{Dt}\right) \tag{10}$$

The vorticity field is discretized by vortex elements. A vortex element proposed for single-phase flow simulation[24] is employed. The vortex element has a viscous core, and the vorticity distribution around the element is represented with the Gaussian curve. When the vortex element γ at $\boldsymbol{x}^\gamma$ is supposed to have a circulation Γ_γ and a core radius σ_γ, the vorticity at $\boldsymbol{x}$ induced by the element is expressed as:

$$\omega^\gamma(\boldsymbol{x}) = \frac{\Gamma_\gamma}{\pi\sigma_\gamma^2}\exp\left[-\left(\frac{|\boldsymbol{x}-\boldsymbol{x}^\gamma|}{\sigma_\gamma}\right)^2\right] \tag{11}$$

The convection of the vortex element γ is estimated by the Lagrangian calculation of the following equation.

$$\frac{d\boldsymbol{x}^\gamma}{dt} = \boldsymbol{u}_l(\boldsymbol{x}^\gamma) \tag{12}$$

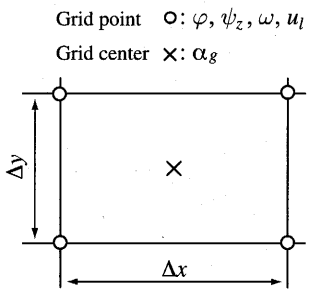

Fig. 1 Computational grid

The computational domain in the x–y plane is resolved into rectangular grids. A grid is shown in Fig. 1. The scalar potential ϕ, the z-component for vector potential ψ_z, the vorticity ω and the liquid velocity $\boldsymbol{u}_l$ are defined on the grid points. ϕ and ψ_z are computed from Eqs. (8) and (9) respectively, and $\boldsymbol{u}_l$ is calculated from Eq. (6). When solving Eq. (9) for ψ_z, the ω value on the grid points is determined by taking the summation of the vorticities produced by every vortex element. The α_l value in Eq. (8) is estimated from Eq. (3) after computing the volumetric fraction for the gas-phase α_g from the Lagrangian calculation of Eq. (4). When the bubbles are assumed to distribute uniformly with an interval Δz in the z-direction normal to the x–y plane at the inlet of computational domain, the α_g value for a grid with an area A ($=\Delta x\Delta y$) is expressed as:

$$\alpha_g = \frac{(\pi/6)d^3 n_g}{A\Delta z} \tag{13}$$

where n_g is the number of bubbles in the grid.

It is found from Eq. (10) that the vorticity varies with the lapse of time due to the viscous diffusion and the gradient of the volumetric fraction. These variations are considered through the changes in σ and Γ for the vortex element, and they are computed simultaneously with the Lagrangian calculation of Eq. (12).

3.2 Change in core radius due to viscosity

The vorticity decreases due to the viscous effect. For the single-phase flow analysis, the decrement is simulated by applying a core spreading method[24], in which the core radius of vortex element is made to increase with the lapse of time. This study applies the method to the two-phase flow analysis, and the time variation for the core radius is evaluated through the Lagrangian calculation of the following equation.

$$\frac{d\sigma}{dt} = \frac{2\nu_l}{\alpha_l\sigma} \tag{14}$$

where the superficial value ν_l/α_l is used as the kinematic viscosity in due consideration of the first term on the right-hand side for Eq. (10).

3.3 Change in circulation due to bubble motion

When employing the Reynolds transport theorem, the time rate of change in the circulation Γ along any closed curve (surface element dS) is expressed by the following equation.

$$\frac{D\Gamma}{Dt} = \int_S \left[\frac{\partial \omega}{\partial t} + \nabla \cdot (\omega \boldsymbol{u}_l) \right] dS \qquad (15)$$

Substituting Eq. (10) into the integrand of Eq. (15), the following relation is derived:

$$\frac{D\Gamma}{Dt} = \int_S \left[\frac{1}{\alpha_l} \nabla \alpha_l \times \left(\boldsymbol{g} - \frac{D\boldsymbol{u}_l}{Dt} \right) \right] dS \qquad (16)$$

where the viscous diffusion term is omitted because it is already considered by Eq. (14).

The application of Eq. (16) to the above-mentioned computational grid yields the time rate of change in Γ, $\Delta\Gamma/\Delta t$, in the grid. The numerical integration is performed by postulating that the integrand of Eq. (16) varies linearly between the grid points. In the case that the number of vortex elements in a grid is n_v, the change in the circulation for each vortex element during Δt is supposed to be $\Delta\Gamma/n_v$. In the case that there are no vortex elements in the grid, a vortex element with a circulation $\Delta\Gamma$ is generated at the center of the grid.

3.4 Numerical procedure

When the flow field at $t = t$ is known, the flow at $t = t + \Delta t$ is estimated by the following procedure.

1. Simulate the bubble motion from Eq. (4).
2. Calculate α_g from Eq. (13) to estimate α_l from Eq. (3).
3. Calculate σ from Eq. (14)
4. Calculate $\Delta\Gamma$ from Eq. (16).
5. Simulate the convection of vortex element from Eq. (12) to calculate ω from Eq. (11).
6. Calculate ψ from Eq. (9).
7. Calculate ϕ from Eq. (8).
8. Calculate $\boldsymbol{u}_l$ from Eq. (6).

4. Application to Bubbly Flow Analysis around a Cylinder

4.1 Simulation conditions

The present method is applied to simulate the air-water bubbly flow around a square-section cylinder. The flow was experimentally investigated by Shakouchi et al.[5),6)]. The square-section cylinder, of which side length s is 30 mm, is mounted in a channel with 90 mm × 45 mm cross-sectional area. The flow direction is vertically upward. The Reynolds number Re, based on s and the water velocity u_{l0} upstream of the cylinder, is 15 000.

Figure 2 shows the computational domain. The inlet and outlet boundaries, B_0 and B_3, are located $3s$ upstream and $10.3s$ downstream of the cylinder, respectively. The domain is resolved into 18×80 square grids.

The vorticity field is generated by the bubble motion and the velocity shear layer originating from the cylinder surface. The vorticity field due to the velocity shear layer is simulated by a method presented by Kamemoto and Miyasaka[25] for single-phase flow analysis. The vorticity layer on the cylinder is divided into segments with a length l along the cylinder surface, and a vortex element

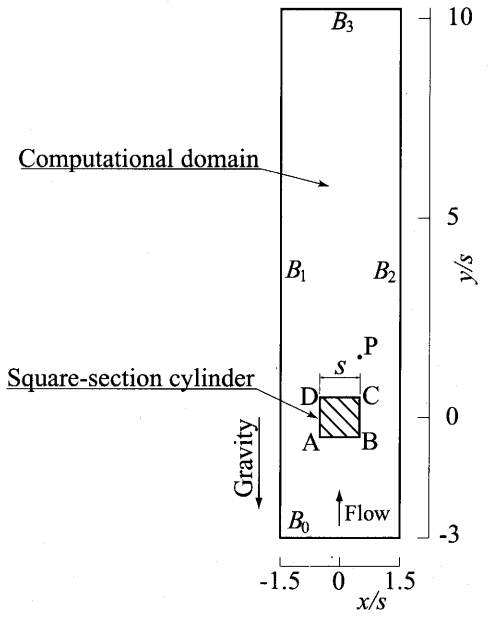

Fig. 2 Computational domain

is released from each segment into the flow field at a time interval Δt. In this simulation, the number of segments is 96, and the height of vorticity layer h is set at $5/Re^{1/2}$ with reference to the single-phase flow analysis[25]. When releasing the vortex element, the strength is equivalent to the vorticity in the segment and the core radius σ_0 is determined from the relation $\pi\sigma_0^2 = lh$. The σ_0 value for the vortex element used to represent the vorticity field caused by the bubble motion is the grid size Δx in the x-direction. The vortex element leaving the outlet boundary B_3 is excluded from the calculation. To consider the exclusion, a region with a length $3s$ is added downstream of B_3 and the vortex elements are made to convect in the region with their velocity kept constant. The vorticity layer on the channel wall can also be represented through the same method applied on the cylinder surface. Assuming that the vorticity layer scarcely affects the wake of the cylinder, it is ignored and the slip condition for velocity is imposed on the channel wall.

The bubbles are released with a velocity u_{g0} from the inlet boundary B_0. Ten bubbles are released at a time interval $2\Delta t$. The diameter is set at the measured value 2.5 mm, and the velocity u_{g0} is estimated from the drift flux model[26]. The corresponding experiments[5),6)] reported that dispersed bubbles are observed to flow in the region upstream of the cylinder. To reproduce such bubbly flow condition, the bubble releasing positions are determined by using random numbers. The water single-phase flow is simulated when the nondimensional time $t^* < 7.5$, and the bubbles are released at $t^* \geq 7.5$. It is considered that the bubble shape becomes nonspherical owing to the shear flow around the cylinder. The Lagrangian calculations for the bubble motion and deformation may heighten

the accuracy of the analysis. As the present study aims to propose a vortex method for bubbly flow, the bubble shape is assumed to be spherical, and accordingly the relation $C_V = C_L = 0.5$ is employed in Eq. (4). The Δz value in Eq. (13) is determined so as to satisfy the air volumetric fraction α_{g0} at B_0.

The second-order Adams-Bashforth method is used for the Lagrangian calculation, and the time increment Δt is set at $u_{l0}\Delta t/s = 0.03$. The simulation is performed for $0 \le \alpha_{g0} \le 0.03$. The air volumetric flux J_g determined from the Δz value at $\alpha_{g0} = 0.03$ is 0.91 times larger than that for the experiment, indicating that J_g is nearly parallel to the experimental condition.

The quasi-harmonic equation for ϕ, Eq. (8), and the Poisson equation for the z-component ψ_z of $\boldsymbol{\psi}$, Eq. (9), are solved by the SOR method. The boundary conditions for the water are given as follows; the uniform velocity u_{l0} on the inlet boundary B_0, the convective outflow condition on the outlet boundary B_3, and the slip condition on the channel walls B_1 and B_2. Therefore, the boundary conditions for ϕ and ψ_z are expressed as follows.

$$\frac{\partial \phi}{\partial y} = u_{l0}, \quad \frac{\partial \psi_z}{\partial y} = 0 \quad \text{on} \quad B_0 \tag{17}$$

$$\frac{\partial \phi}{\partial y} = u_{l0}, \quad \text{on} \quad B_3 \tag{18}$$

$$\frac{\partial \phi}{\partial x} = 0, \quad \frac{\partial \psi_z}{\partial x} = 0 \quad \text{on} \quad B_1 \text{ and } B_2 \tag{19}$$

The Sommerfeld radiation condition is imposed for ψ_z on the boundary B_3, where the mean velocity on B_3 is used for the phase velocity[27]. On the cylinder surface ABCD, the following conditions are imposed to satisfy the non-slip condition.

$$\frac{\partial \phi}{\partial x} = 0, \quad \frac{\partial \psi_z}{\partial x} = u_{l0} \quad \text{on AB and CD} \tag{20}$$

$$\frac{\partial \phi}{\partial y} = u_{l0}, \quad \frac{\partial \psi_z}{\partial y} = 0 \quad \text{on AD and BC} \tag{21}$$

The pressure is calculated from the Poisson equation derived by taking the divergence of Eq. (2).

4.2 Results for water single-phase flow

Figure 3 shows the time variation for the number of vortex elements N_v in the computational domain. For the water single-phase flow analysis, N_v varies almost periodically around 15 400 at $t^* \ge 40$. This demonstrates that the time-averaged number of the vortex elements generated from the cylinder surface balances that of the elements flowing out of the domain. Accordingly, a fully developed water single-phase flow appears at $t^* \ge 40$.

The flow fields at $t^* = 100$ are shown in Fig. 4. The vortex elements released from the cylinder surface are plotted by the symbol ∘ in Fig. 4 (a). They form clusters downstream of the cylinder, and the clusters flow downstream at an even interval. Figure 4 (b) shows the velocity distribution, where the velocity upstream of the cylinder u_{l0} is subtracted to make the vortical structure more understandable. The large-scale eddies or the Karman vortices correspond to the clusters of vortex element. The vortex shedding frequency agrees well with the measured result[5], as discussed later.

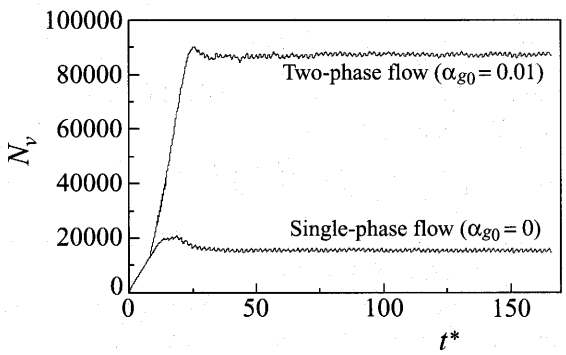

Fig. 3 Time variation for number of vortex elements

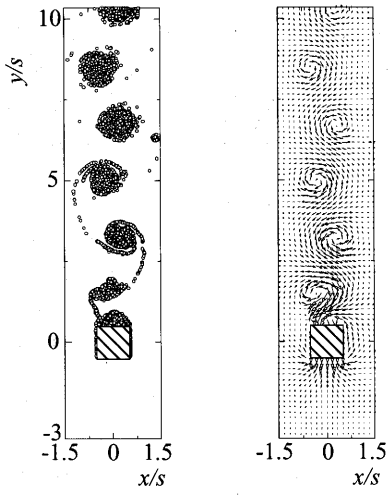

(a) Vortex element (b) Velocity

Fig. 4 Water single-phase flow field at $t^* = 100$

Figure 5 shows the pressure distribution at the same instant as Fig. 4. The distribution for the pressure coefficient C_p is plotted, where the static pressure is excluded. The pressure reaches its maximum value at the front of the cylinder, and it takes the minimum one at the center of Karman vortex.

4.3 Results for bubbly flow

The time variation for the number of vortex elements N_v for the bubbly flow is superimposed in Fig. 3. The air volumetric fraction α_{g0} at the inlet boundary is 0.01. The bubbles are released when $t^* \ge 7.5$. N_v varies periodically around 86 500 at $t^* \ge 40$, demonstrating the appearance of a fully developed bubly flow. The N_v value for the bubbly flow is about 5.6 times larger than that for the water single-phase flow. This is because a number of vortex elements are introduced to represent the vorticity field induced by

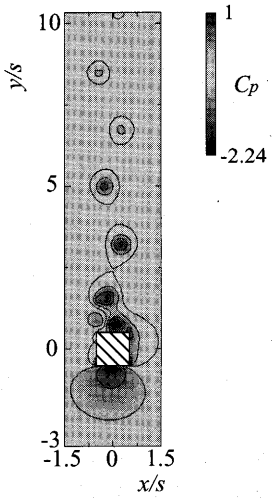

Fig. 5 Pressure distribution for water single-phase flow at $t^* = 100$

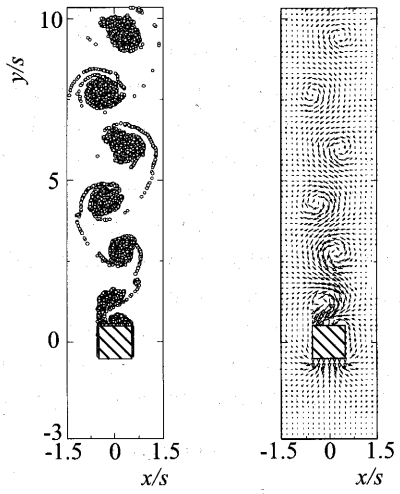

(a) Vortex element (b) Water velocity

Fig. 6 Two-phase flow field at $t^* = 84$ in case of $\alpha_{g0} = 0.01$

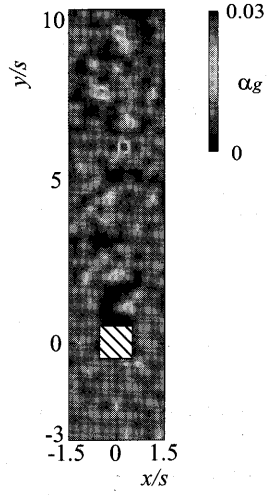

Fig. 7 Distribution of air volumetric fraction at $t^* = 84$ in case of $\alpha_{g0} = 0.01$

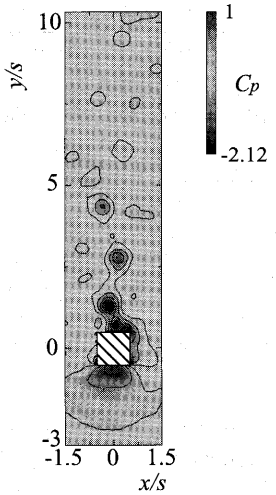

Fig. 8 Pressure distribution at $t^* = 84$ in case of $\alpha_{g0} = 0.01$

the bubble motion. The computation was performed on a personal computer with a Pentium 4 processor. The calculation at $0 \le t^* \le 150$ for the water single-phase flow required 16.9 hours, and that for the two-phase flow of $\alpha_{g0} = 0.01$ required 73.7 hours.

Figure 6 presents the bubbly flow fields at $t^* = 84$, where $\alpha_{g0} = 0.01$. The vortex elements introduced from the cylinder surface distribute as shown in Fig. 6 (a). They form clusters similar to those for the water single-phase flow (Fig. 4 (a)). The vortex elements, generated by the bubble motion, distribute in the whole region, though their depiction is omitted. Figure 6 (b) shows the water velocity distribution. Comparing with the distribution for the single-phase flow (Fig. 4 (b)), the Karman vortex becomes unclear. It is found that the strength reduces.

Figure 7 shows the distribution for the air volumetric fraction α_g at the same instant as Fig. 6. The bubbles are hardly found just behind the cylinder. Such bubble distribution was also observed in the experiment[5]. As the bubbles are entrained into the Karman vortex, where the pressure reaches its minimum value, α_g takes its maximum value at the center of Karman vortex. The maximum value is about three times larger than the air volumetric fraction upstream of the cylinder. The decrement in the strength of Karman vortex indicated in Fig. 6 (b) is due to the bubble entrainment.

The pressure distribution at the same instant as Figs. 6 and 7 is shown in Fig. 8. The distribution in the region upstream of the cylinder is nearly the same as that for the single-phase flow presented in Fig. 5. But the minimum pressure at the center of Karman vortex is higher. The reduction for the strength of Karman vortex found in Fig. 6 is also confirmed from the pressure distribution. Such relaxation of pressure gradient and reduction for strength of large-scale eddies due to the bubble entrainment were also reported by Ruetsch and Meiburg[9] performing the DNS of a plane mixing layer.

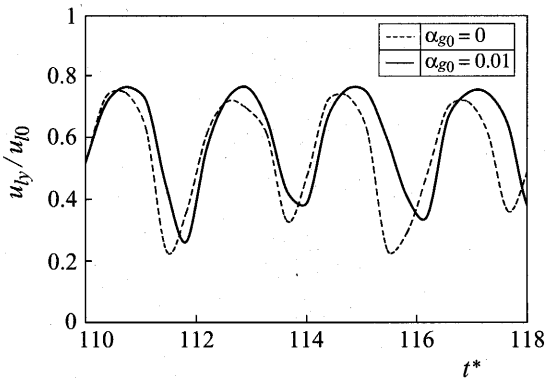

Fig. 9 Time variation of water velocity at point P

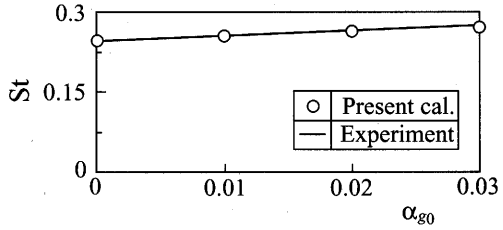

Fig. 10 Vortex shedding frequency

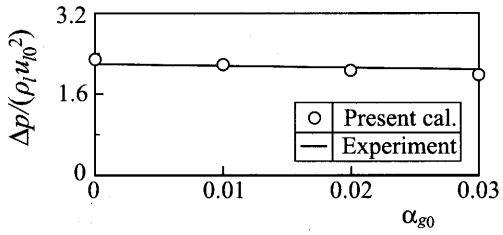

Fig. 11 Pressure difference between front and rear stagnation points of cylinder

When the vertical velocity of water u_{ly} is calculated at a point P indicated in Fig. 2, it varies almost periodically as shown in Fig. 9. The point P is located s downstream of the cylinder rear edge. The variation is caused by the passing of the Karman vortex. The velocity for the two-phase flow ($\alpha_{g0}=0.01$) is slightly higher than that for the single-phase flow. This suggests that the present simulation captures successfully the accerelation of water due to the buoyancy effect of the entrained bubbles.

Estimating the shedding frequency of Karman vortex f from the time variation of the water velocity at the point P, the Strouhal number St changes as the function of α_{g0} as plotted in Fig. 10. St becomes higher with increasing α_{g0}. This is caused by the increment in the water velocity shown in Fig. 9. The simulated result agrees well with the experiment[5].

The pressure difference Δp between the front and rear stagnation points of the cylinder is shown in Fig. 11. The Δp value reduces with increasing α_{g0} at $\alpha_{g0} \leq 0.03$, being in agreement with the experiment[6]. The reduction may be attributable to the decrement in the mean density for the

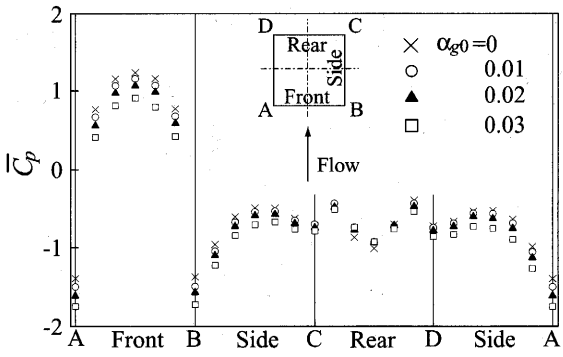

Fig. 12 Pressure distribution on cylinder

two-phase mixture. The reduction of Δp due to the increment in α_{g0} is slightly larger than that for the experiment. This is owing to the fact that the increment in α_{g0} reduces more the pressure at the front of the cylinder. Because the strong shear flow exists near the cylinder, and therefore the bubble motion is not sufficiently captured when the bubble shape is assumed to be spherical.

The pressure distribution on the cylinder surface is presented in Fig. 12, where the time-averaged pressure coefficient $\overline{C_p}$ is plotted. $\overline{C_p}$ takes its maximum value at the center of the front surface, and it is low on the side and rear surfaces. It decreases with increasing α_{g0}. But the $\overline{C_p}$ value on the rear surface is hardly independent of α_{g0}. This is because the bubbles scarcely exist just behind the cylinder, as found in Fig. 7. These changes in $\overline{C_p}$ caused by the increment in α_{g0} are favorably compared with the measurement[6], though the depiction is omitted.

5. Conclusions

A two-dimensional vortex method for gas-liquid two-phase free turbulent flow is proposed. It is based on the Vortex in Cell method, in which the scalar potential and the vector potential are solved to calculate the liquid velocity. The behavior of vortex element and the bubble motion are calculated through the Lagrangian approach, while the change in the vorticity due to the bubble is analyzed in the computational grids resolving the flow field.

The vortex method is also applied to simulate the air-water bubbly flow around a square-section cylinder. The flow direction is vertically upward, and the air volumetric fraction α_{g0} upstream of the cylinder ranges from 0 to 0.03. The simulated flow features, such as the preferential concentration of bubble in the Karman vortex, the resultant reduction for the strength of vortex and the relaxation for the pressure gradient, are favorably compared with the existing numerical results on the bubble-laden free turbulent flows. It is also confirmed that the shedding frequency for Karman vortex and the pressure distribution on the cylinder agree well with the measurement. These indicate the validity of the present method.

Acknowledgement

This study was partially supported by a Grant-in-Aid for the 21st Century COE Program "Frontiers of Computational Science" from the Ministry of Education, Culture, Sports, Science and Technology of Japan.

References

(1) Roig, V., Suzanne, C. and Masbernat, L., Experimental Investigation of a Turbulent Bubbly Mixing Layer, Int. J. Multiphase Flow, Vol.24, No.1 (1998), pp.35–54.

(2) Rightley, P.M. and Lasheras, J.C., Bubble Dispersion and Interphase Coupling in a Free-Shear Flow, J. Fluid Mech., Vol.412 (2000), pp.21–59.

(3) Sun, T.Y. and Faeth, G.M., Structure of Turbulent Bubbly Jets-I. Methods and Centerline Properties, Int. J. Multiphase Flow, Vol.12, No.1 (1986), pp.99–114.

(4) Inoue, A., Kozawa, Y., Yokosawa, M. and Aoki, S., Studies on Two-Phase Cross Flow, Part I: Flow Characteristics around a Cylinder, Int. J. Multiphase Flow, Vol.12, No.2 (1986), pp.149–167.

(5) Shakouchi, T., Tian, D. and Ida, T., Behavior of Vertical Upward Gas-Liquid Bubbly Flow Past Obstacle in Rectangular Channel (Effect of Blockage Ratio), JSME Int. J., Ser.B, Vol.45, No.3 (2002), pp.686–6932.

(6) Shakouchi, T., Tian, D., Ida, T. and Nakamura, T., Behavior of Flow around Obstacle in Vertical Gas-Liquid, Bubbly Two-Phase Flow (Effects of Geometry and Aspect Ratio of Obstacle), Trans. Jpn. Soc. Mech. Eng., (in Japanese), Vol.68, No.672, B (2002), pp.2240–2246.

(7) Sun, T.Y. and Faeth, G.M., Structure of Turbulent Bubbly Jets-II. Phase Property Profiles, Int. J. Multiphase Flow, Vol.12, No.1 (1986), pp.115–126.

(8) Sugiyama, K., Takagi, S. and Matsumoto, Y., Three Dimensional Numerical Analysis for Bubbly Flow around a Circular Cylinder, JSME Int. J., Ser.B, Vol.44, No.3 (2001), pp.319–327.

(9) Ruetsch, G.R. and Meiburg, E., Two-Way Coupling in Shear Layers with Dilute Bubble Concentrations, Phys. Fluids, Vol.6, No.8 (1994), pp.2656–2670.

(10) Druzhinin, O.A. and Elghobashi, S.E., Direct Numerical Simulation of a Three-Dimensional Spatially Developing Bubble-Laden Mixing Layer with Two-Way Coupling, J. Fluid Mech., Vol.429 (2001), pp.23–61.

(11) Uchiyama, T. and Naruse, M., A Numerical Method for Gas-Solid Two-Phase Free Turbulent Flow Using a Vortex Method, Powder Technol., Vol.119 (2001), pp.206–214.

(12) Uchiyama, T. and Fukase, A., Three-Dimensional Vortex Method for Gas-Particle Two-Phase Compound Round Jet, Trans. ASME, J. Fluid Eng., Vol.127 (2005), pp.32–40.

(13) Uchiyama, T. and Naruse, M., Numerical Simulation of Gas-Particle Two-Phase Mixing Layer by Vortex Method, Powder Technol., Vol.125 (2002), pp.111–121.

(14) Uchiyama, T. and Naruse, M., Vortex Simulation of Slit Nozzle Gas-Particle Two-Phase Jet, Powder Technol., Vol.131 (2003), pp.156–165.

(15) Uchiyama, T. and Yagami, H., Numerical Analysis of Gas-Particle Two-Phase Wake Flow by Vortex Method, Powder Technol., Vol.149 (2005), pp.112–120.

(16) Uchiyama, T. and Naruse, M., Three-Dimensional Vortex Simulation for Particulate Jet Generated by Free Falling Particles, Chem. Eng. Sci., Vol.61 (2006), pp.1913–1921.

(17) Uchiyama, T. and Fukase, A., Three-Dimensional Vortex Simulation of Particle-Laden Air Jet, Chem. Eng. Sci., Vol.61 (2006), pp.1767–1778.

(18) Uchiyama, T. and Naruse, M., Numerical Simulation of Gas-Particle Two-Phase Free Turbulent Flow Based on Vortex in Cell Method, Powder Technol., Vol.142 (2004), pp.192–208.

(19) Sene, K.J., Hunt, J.C.R. and Thomas, N.H., The Role of Coherent Structures in Bubble Transport by Turbulent Shear Flows, J. Fluid Mech., Vol.259 (1994), pp.219–240.

(20) Uchiyama, T., Three-Dimensional Vortex Simulation of Bubble Dispersion in Excited Round Jet, Chem. Eng. Sci., Vol.59 (2004), pp.1403–1413.

(21) Yang, X., Thomas, N.H., Guo, L.J. and Hou, Y., Two-Way Coupled Bubble Laden Mixing Layer, Chem. Eng. Sci., Vol.57 (2002), pp.555–564.

(22) Schiller, L. and Naumann, A.Z., Über die Grundlegenden Berechungen bei der Schwerkraftaufbereitung, Zeit. Vereines Inge., Vol.77 (1933), pp.318–321.

(23) Hirasaki, G.J. and Hellums, J.D., Boundary Conditions on the Vector and Scalar Potentials in Viscous Three-Dimensional Hydrodynamics, Quart. Appl. Math., Vol.28, No.2 (1970), pp.293–296.

(24) Leonard, A., Vortex Methods for Flow Simulation, J. Comput. Phys., Vol.37 (1980), pp.289–335.

(25) Kamemoto, K. and Miyasaka, T., Development of a Vortex and Heat Elements Method and Its Application to Analysis of Unsteady Heat Transfer around a Circular Cylinder in a Uniform Flow, VORTEX METHODS, Edited by Kamemoto, K. and Tsutahara, M., (2000), pp.135–144, World Scientific.

(26) Ishii, M., One-Dimensional Drift-Flux Model and Constitutive Equations for Relative Motions between Phases in Various Two Phase Flow Regimes, ANL Report, ANL-77–47, (1977).

(27) Kawakami, K., Nishida, H. and Satofuka, N., An Open Boundary Condition for the Numerical Analysis of Unsteady Incompressible Flow Using the Vorticity-Streamfunction Formulation, Trans. Jpn. Soc. Mech. Eng., (in Japanese), Vol.68, No.574, B (1994), pp.1891–1896.